Lab 2:
Introduction to Shock/Boundary Layer Interaction
AAE 520

Purdue University
School of Aeronautical and Astronautical Engineering

Tom Shaw
Jason Spohn
2/21/05

Introduction to Shock/Boundary Layer Interaction

1. Abstract

Using a small supersonic wind tunnel, three different ramp geometries were used to study flow through an oblique shock and over an expansion fan. By varying the ramp angle, the ramp length, the stagnation pressure and the back pressure, different characteristics of the flow could be examined. Three different methods were used to collect data: digital pressure readings, Schlieren photography method, and oil flow visualization. Each of these methods were used to analyze the differences in the behavior of the flow through the nozzle test section and over the ramp.

2. Introduction

When air flows at supersonic speeds, it can easily traverse corners, unlike a flow at subsonic speed. The F117 shown to the right is designed for supersonic flight. If it were to normally fly at subsonic speeds, the sharp corners would produce significant drag and create large boundary layers which would greatly limit the speed of the aircraft. However, in supersonic flight, the air is able to move around these corners much more easily. However, supersonic shocks occur at various places along the jet, creating drag. Shocks occur anywhere the air is supersonic and is forced to expand or contract. This experiment will study the effect of sharp corners on a supersonic flow; specifically, oblique shocks traversing a converging ramp and the expansion fans associated with the top of the ramp.

3. Background

In order to understand or question the results of the experiment, it is necessary to first understand some basic physics behind shock waves and how they behave in a converging corner. Before that however, it might be of interest to quickly state how a converging-diverging nozzle is used to create a supersonic flow.

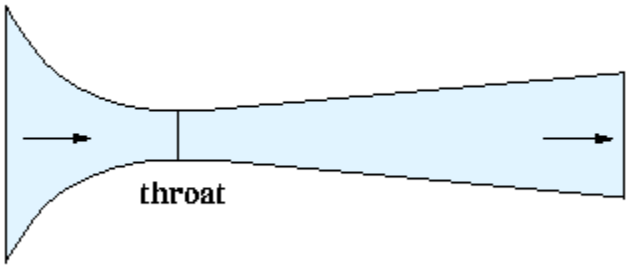

Figure 1: Converging-Diverging Nozzle

The picture to the left represents a converging diverging nozzle. As the air travels thought he nozzle it moves through different characteristic behaviors. As the flow is almost zero in the plenum chamber, the large pressure difference starts the air moving down the tunnel. As the subsonic flow is forced through the converging nozzle, it is sped up. The flow reaches Mach 1, or sonic condition, at the throat. It then enters the diverging nozzle supersonically and is sped up. This is also called choked flow. During choked flow, the pressure downstream of the nozzle has no effect on the mass flow rate of the air coming through the nozzle. However, having a lower backpressure can allow the stagnation pressure to be lower and still achieve supersonic flow.

The super sonic wind tunnel used for this experiment was not able to be run for long periods of time. This is due to the way the wind tunnel creates the supersonic flow. The tunnel operates using a high pressure chamber and a low pressure chamber. The low pressure chamber could be kept at atmospheric or lowered to near vacuum conditions. This affects the speed of the air flow until it becomes supersonic, or choked. After that point, changing the back pressure does not increase the air speed. The plenum pressure can be changed to increase or decrease the stagnation pressure and change the air density. Because the wind tunnel relies on a fixed volume of pressurized air to operate, the time for each test was limited to 20 seconds.

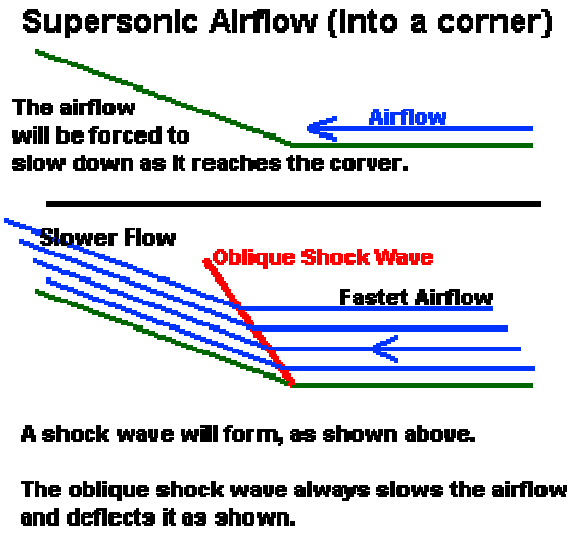

When supersonic air is subjected to a corner, a shock wave will form. The shock will slow the air down as air flows through it, but only the component in the direction perpendicular to the shock wave. The component of velocity parallel to the shock is unaffected. This causes the air to deflect as it enters the shock. The result is an airflow that easily changes directions around corners, as opposed to subsonic flow where a sharp corner creates a large boundary layer and separation.

Figure 2: Supersonic Airflow Through Oblique Shock

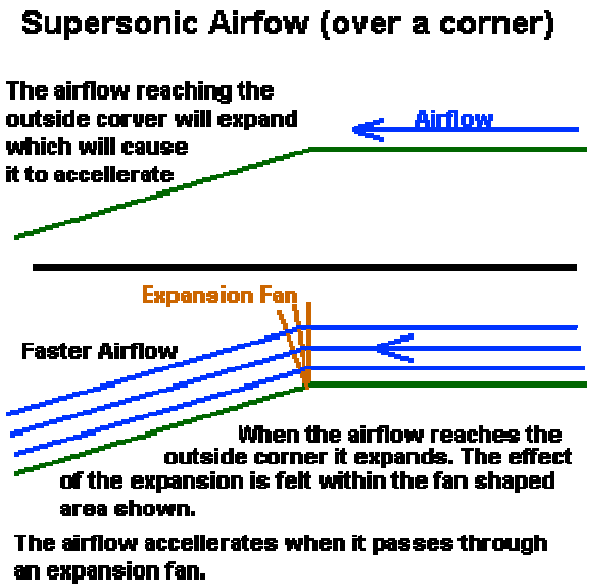

The air flowing into a diverging corner is affected differently. At supersonic speeds, the air speed increases as it goes through the expansion fan created at the corner. For subsonic speeds, this type of corner would decrease the airspeed because no expansion fan would be created. Once the air is through the expansion fan, it stops accelerating and the speed is again constant.

Figure 3: Supersonic Airflow Through Expansion Fan

Equations 1 through 3 are used to calculate the Mach number in the test section of the tunnel where P is pressure, T is temperature, M is Mach number, A is the cross section area, and γ is the ratio of specific heats. These values are all for a point along the length of the nozzle. Equation 4 is used to calculate the oblique shock angle β where θ is the ramp angle. Equation 5 is used to calculate the Mach number between the shock and the expansion fan. Equation 6 relates the total pressure before a shock to the total pressure after the shock and equation 7 calculates the increase in Mach number as flow goes over an expansion fan.

$$\frac{P_o}{P} = \left(1 + \frac{\gamma - 1}{2} M^2\right)^{\frac{\gamma}{\gamma - 1}} \quad \textbf{(1)}$$

$$\frac{T_o}{T} = 1 + \frac{\gamma - 1}{2} M^2 \quad \textbf{(2)}$$

$$\left(\frac{A}{A^*}\right)^2 = \frac{1}{M^2}\left[\frac{2}{\gamma + 1}\left(1 + \frac{\gamma - 1}{2} M^2\right)\right]^{\frac{\gamma + 1}{\gamma - 1}} \quad \textbf{(3)}$$

$$\cot(\theta) = \tan(\beta)\left[\frac{6M_1^2}{5\left(M_1^2 \sin^2(\beta) - 1\right)} - 1\right] \quad \textbf{(4)}$$

$$M_2^2 \sin^2(\beta-\theta) = \frac{1+\frac{\gamma-1}{2}M_1^2 \sin^2\beta}{\gamma M_1^2 \sin^2\beta - \frac{\gamma-1}{2}} \quad \textbf{(5)}$$

$$\frac{P_{02}}{P_{01}} = \left[\frac{6M_1^2\sin^2(\beta)}{M_1^2\sin^2(\beta)+5}\right]^{\frac{7}{2}}\left[\frac{6}{7M_1^2\sin^2(\beta)-1}\right]^{\frac{5}{2}} \quad \textbf{(6)}$$

$$\nu(M) = \sqrt{\frac{\gamma+1}{\gamma-1}}\tan^{-1}\sqrt{\frac{\gamma-1}{\gamma+1}(M^2-1)} - \tan^{-1}\sqrt{(M^2-1)} \quad \textbf{(7)}$$

4. Objectives

The goals of this experiment were to learn to use the supersonic wind tunnel and all associated equipment as well as perform some explorative tests of shocks and boundary layers formed by various ramp geometries. Three main tests were run during this experiment, each with several sets of data collected.

1. Examine the effect of ramp geometry on the formation and shape of the shock and boundary layer produced by the ramp at a given speed. Both pressure data along the ramp and Schlieren images were collected as data for three different ramps.

2. Examine the effect of stagnation pressure on the formation and shape of the shock and boundary layer produced by the ramp. Pressure and Schlieren images were collected for various stagnation pressures. All three ramps were used for this test.

3. Using oil flow visualization, attempt to understand the formation of the boundary layer and shock by; determining where the shock occurs, what angle the shock forms at, how does this affect the flow close to the shock, and identifying any 2D effects observed in the flow.

5. Procedure

5.1 Setting up the Wind Tunnel

The wind tunnel, as discussed in the background section, creates high speed flow by creating a high pressure differential using compressed air and vacuum pressure. This allows a very short test duration before the pressure differential starts to fall. The tunnel is shown in Figure 4. Three methods of data collection were used in this experiment. Pressure data was collected via pressure tubes connected to a digital pressure transducer and read into a computer where it was recorded electronically. This was crucial as it is not possible to collect the data from each tube manually in the 20s allotted per test. The Schlieren method was also used in this experiment to visualize the oblique shock and

expansion fan created by the ramps. The setup of this system is depicted in Figure 5. Oil flow visualization was also utilized in this experiment as another means of flow visualization. This will be discussed further in the results section.

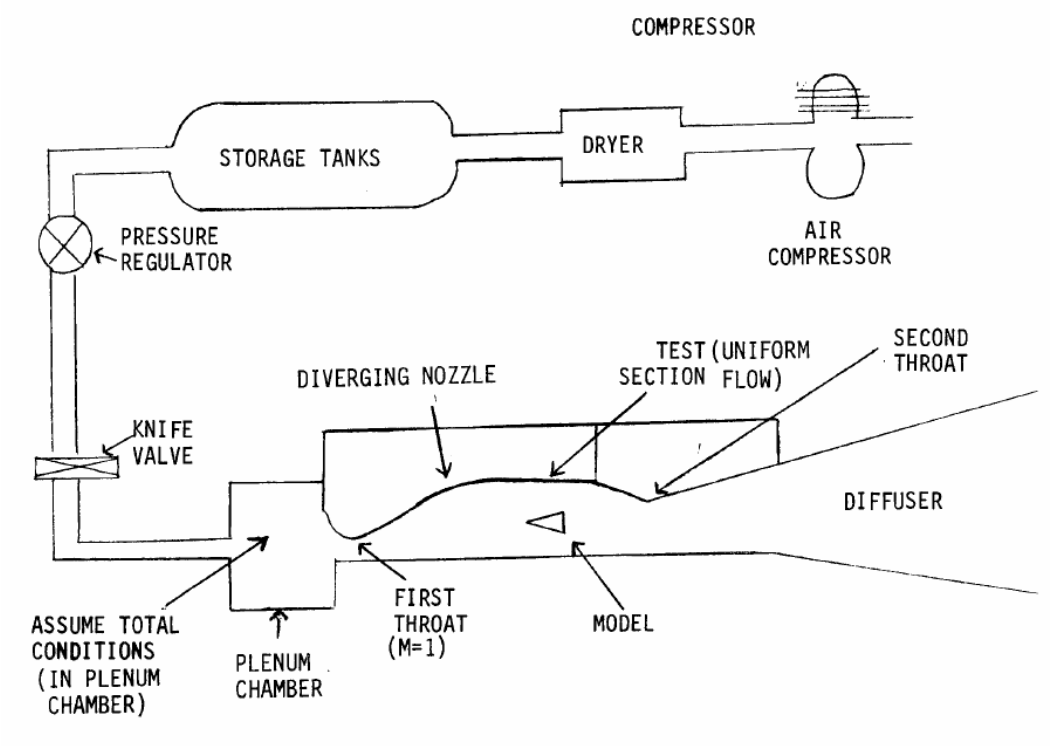

Figure 4: Subsonic Wind Tunnel

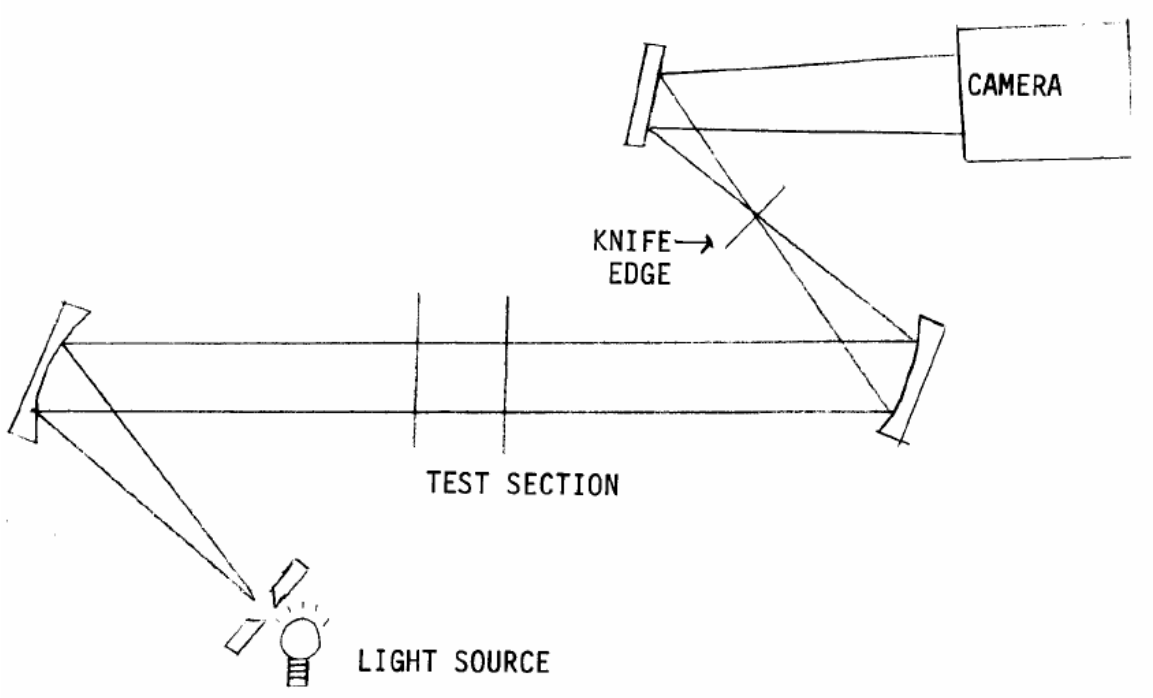

Figure 5: Schlieren Setup

5.2 Initial Pressure Readings

On both tests dates, the tunnel was run empty, without a ramp, before any experiments were conducted. This was to measure the pressure at various points along the nozzle and test section. These pressure readings were used to calculate the mach numbers for the flow at the corresponding tunnel locations and could then be compared to the theoretical values. The tunnel ran at 53 psi gage on the first day while the initial pressure data was collected and 59 psi gage the second day. Given the method of plenum pressure adjustment, a potentiometer, it was difficult to accurately set the plenum pressure to a desired number; thus the 6 psi difference in plenum pressure between days one and two.

5.3 Ramp Pressure Measurements

For each test 1 through 3, the following procedure for measuring the ramp pressures was used.

The test body was screwed into the fixture. The plastic caps were removed from the desired pressure taps and a tube from the digital pressure transducer was connected to each tap being used in the test. The test body was then inserted into the tunnel and tightened down. The desired upstream and downstream pressures were set and allowed to reach equilibrium. The knife valve was then opened and a few seconds were allowed before measurements were taken for the flow to reach equilibrium. The temperature was recorded when it reached a peak temperature and the plenum pressure was recorded. The pressure data was collected and the Schlieren image was digitally stored. All of this data was collect in about 5 seconds for each of the following tests.

1. The longitudinal pressures were measured first, followed by the transverse pressures. Each test was run twice to get an estimation of the fluctuations in the measurements. This was done for a 15° ramp, a 25° ramp and a taller 25° ramp for a total of 12 sets of data. The ramp schematics are depicted in Figures A1 through A3 of the Appendix.

2. The stagnation pressure was adjusted and longitudinal and transverse pressures were measured for each ramp for three different stagnation pressures. The downstream pressure was also changed for a constant stagnation pressure to verify no significant change in the flow.

3. An oil-paint mixture was applied to each ramp and run in the wind tunnel for two different stagnation pressures. No digital pressures were recorded for these tests as they were just for visual inspection. Pictures were taken before and after the test to give an idea of the flow characteristics.

6. Analysis of Results

6.1 Tunnel Pressure Readings

The empty tunnel pressure data for both day 1 and day 2 can be seen in Figure 6 along with the error between the two. Because of the difficulty in repeating an exact experimental value of the stagnation pressure, the pressure ratio (static pressure over the stagnation pressure) is compared. The ramp will be operating in the range of 6 to 12 inches downstream of the nozzle throat where it is evident that there are errors of up to 12%. This indicates that static pressure data from day one and day two cannot reasonably be compared against each other without a degree of inaccuracy.

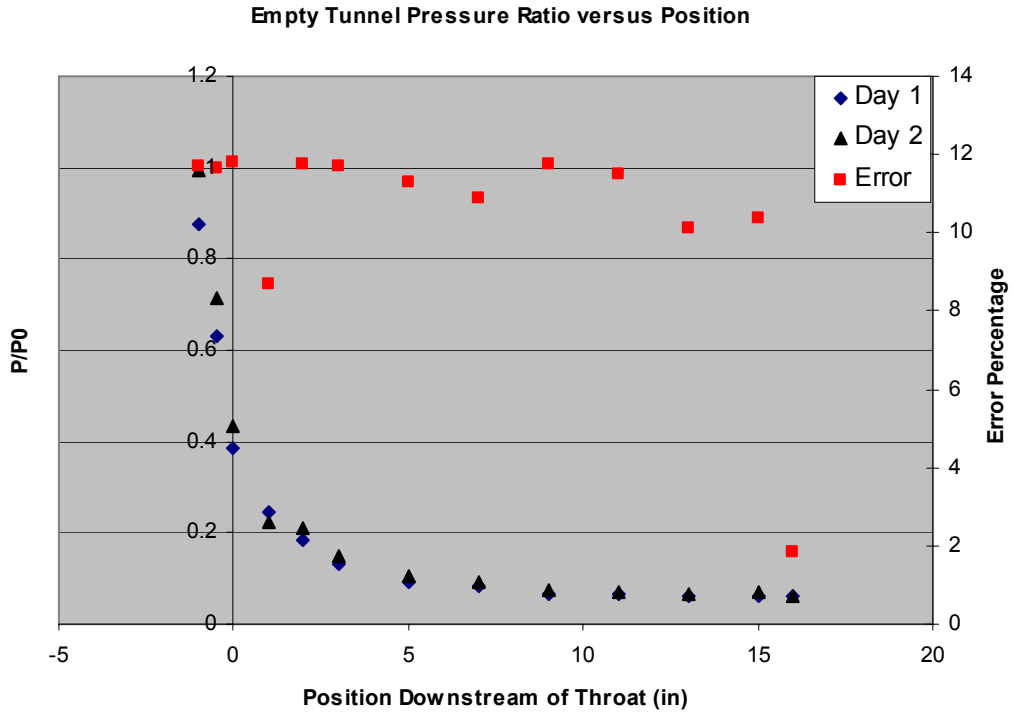

Figure 6: Empty Tunnel Repeatability Comparison

Because the tunnel is empty, there were no shocks being generated in the test section and thus it can be considered isentropic flow. With a constant stagnation pressure, the static pressures can be put into the isentropic pressure ratio formula (equation 1) and the experimental Mach number throughout the tunnel can be found. The theoretical Mach number can be found using the isentropic area ratio formula (equation 3), with the area ratios being defined by the geometry of the nozzle in the lab manual. The experimental versus theoretical Mach number is shown in Figure 7 as well as the relative nozzle geometry. The data follows the expected trends however it also shows a mach number in the test section of 2.35, 8% lower than the theoretical 2.56. This discrepancy can be explained by a buildup of the boundary layer as well as inconsistencies on the walls of the test section. The rough and dirty walls of the wind tunnel can cause a higher shear

force and thus create a larger boundary layer effectively reducing the area of the wind tunnel which in turn reduces the Mach number. The numerous pressure taps on the top wall of the tunnel can create small shocks which will cause a rise in the static which will give a lower than expected Mach number.

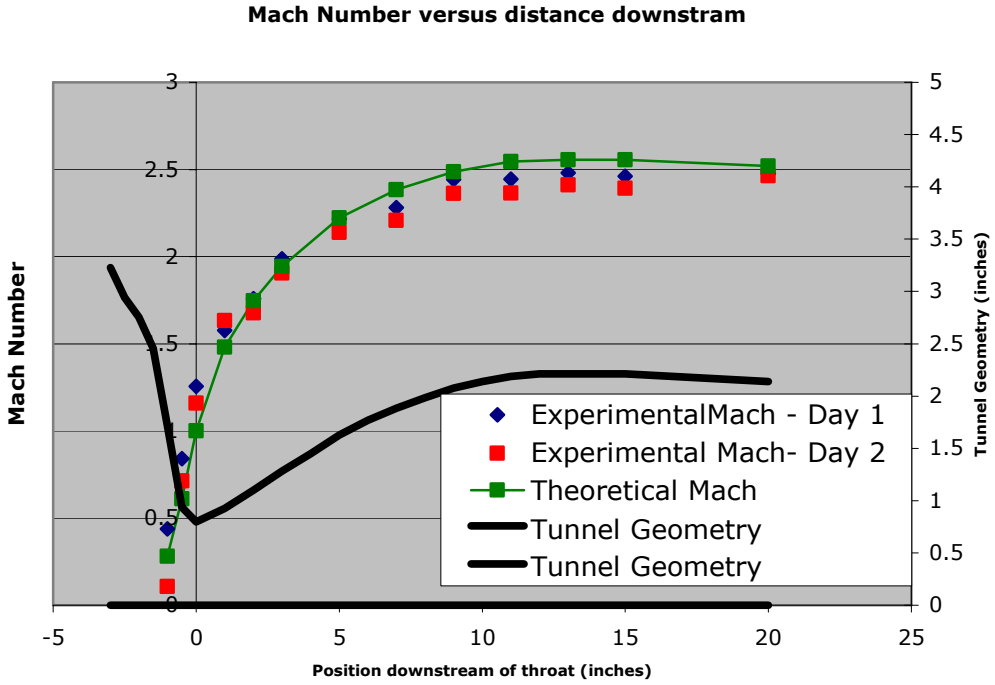

Figure 7: Experimental and Theoretical Tunnel Mach Numbers

6.2 Ramp Geometry Results

The tunnel stagnation pressure was constant for the ramp geometry tests at 53 psig and the ambient temperature and pressure was measured at 76.4 °F and 14.6 psia respectively. The 15° ramp was tested first using longitudinal pressure readings and again using transverse pressure readings. Each test was performed twice to get an idea of the level of flow variation. Therefore, for each ramp, 4 sets of data were gathered. Figure 7 shows the longitudinal pressure data for each ramp along with the corresponding ramp geometry to visualize how the data corresponds to the ramps. The position of the data is defined non-dimensionally as the distance downstream of the beginning of the ramp piece, x, over the entire length of the ramp piece, L, of 5.5 inches. The stagnation pressure of the incoming flow was measured at 67.4 psia, which will be constant only until the flow passes through the compression shock.

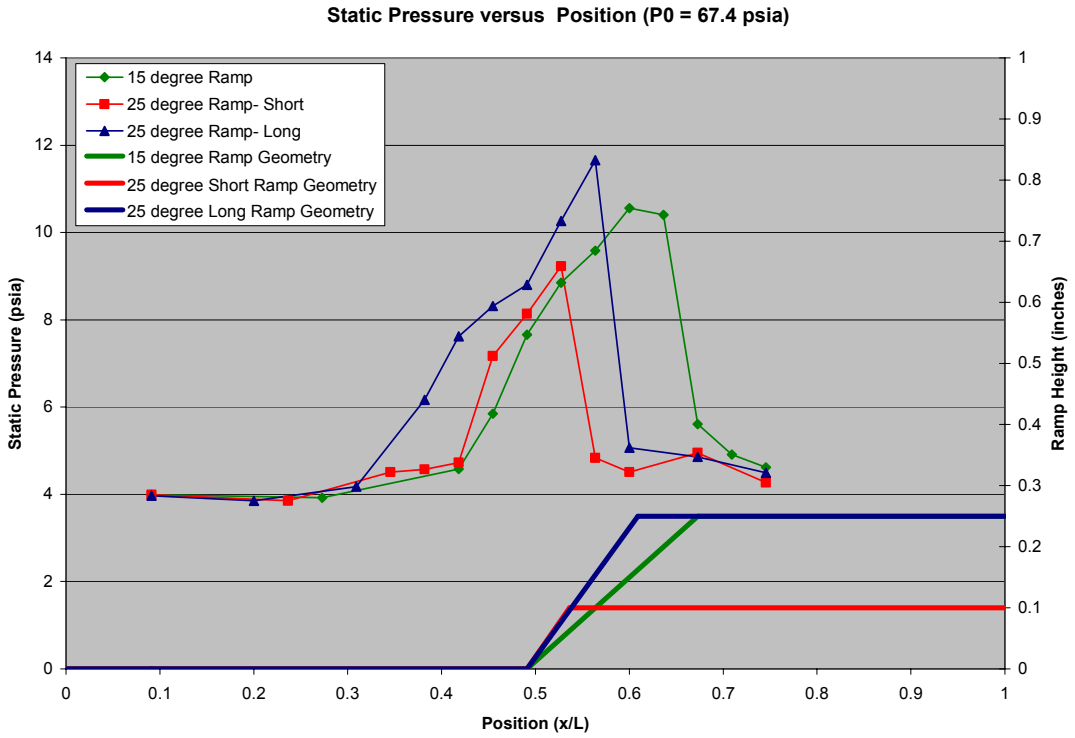

Figure 8: Static Pressure versus Ramp Position

All three pressure distributions follow the expected trend of flow going over a compression ramp and then expansion fan. Before the ramp, the flows for all three cases show identical static pressure as they are all at the same free stream Mach number. As free stream flow hits the oblique shock, the static pressure jumps as the Mach number drops. When the flow is expanded by the expansion fan it is sped up and the Mach number rises as the static pressure falls. This is seen in the plot as the flow drops in static pressure as soon as it turns over the end of the ramp geometry.

It is important to note the significant difference between the points at which the pressure jumps, indicating an oblique shock in the experimental flow, and where the start of the ramp geometry is, indicating where the start of the oblique shock should be. This is due to a separation bubble that is caused by the large corner angles the ramps provide. These separation bubbles are better visualized in the Schlieren images of the flow. Figure 9 shows the 15° ramp during supersonic flow, Figure 10 shows the 25° short ramp, and Figure 11 shows the 25° long ramp. A table of the measured experimental and calculated theoretical shocks angles can be seen in Figure 12. The observed shocks angle was very close for the 15 degree ramp however the two 25 degree ramps gave errors of almost 30%. It is also important to note that the three values of the experimental shock angle are almost identical giving a false speculation that this angle is independent of the ramp angle. However examining the theoretical data shows that the angles should have changed and this inaccuracy is most likely due to the separation bubble that will be discussed shortly.

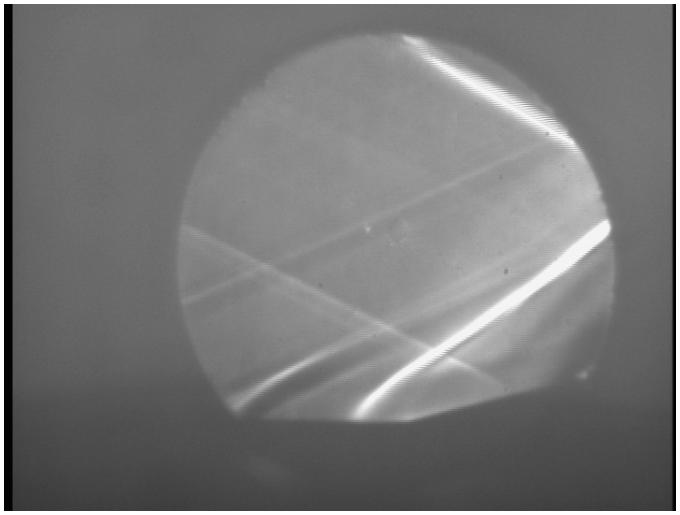

The 15° ramp is shown to the left. It shows a slightly smaller separation bubble than the other ramps. This demonstrates the ramp angle has an effect on the size of the separation bubble as expected. Due to the length of the ramp, the expansion fan is not clearly shown. Oblique shock angle β was calculated from this photograph to be 37.5°.

Figure 9: Schlieren Image of 15° ramp

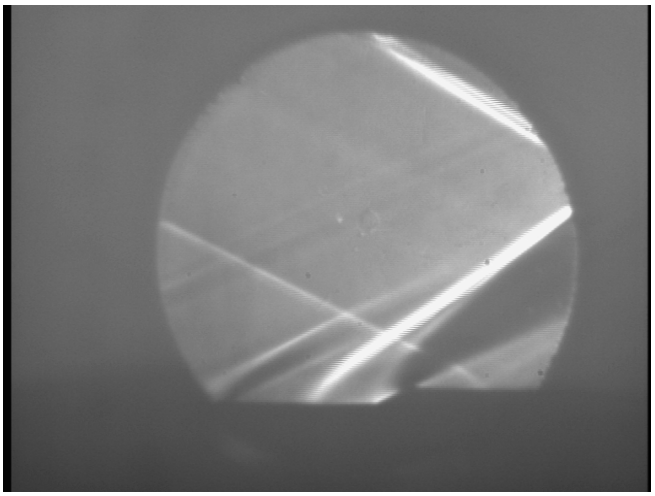

The 25° short ramp clearly shows the expansion fan coming off the top of the ramp. Its separation bubble is slightly larger than the 15° ramp as previously stated. Oblique shock angle β was estimated from this photograph to be 35.5°.

Figure 10: Schlieren Image of 25° short ramp

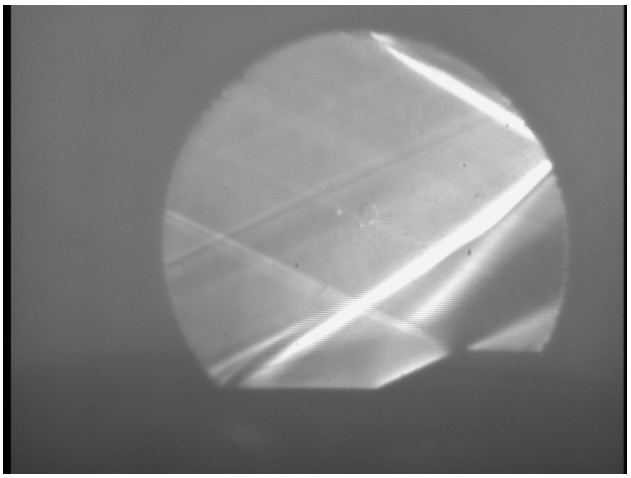

The expansion fan is clearly visible in this picture and the separation bubble is much larger than those for the other two ramps. This suggests the length of the ramp has more of an effect on the bubble size than the angle does. Oblique shock angle β was estimated from this photograph to be 36.0°. However, it appears that the expansion fan is deflecting the shock slightly and has caused an overestimation of the angle.

Figure 11: Schlieren Image of 25° long ramp

Ramp	β_{the}	β_{exp}	Error (%)
15°	36.9	37.5	0.01626
25° Short	50.2	35.5	0.292829
25° Long	50.2	36	0.282869

Figure 12: Experimental Shock Angle Accuracy

As well as examining how the flow changed longitudinally along the ramp, transverse pressure measurements were taken. Transverse pressure data against position can be seen for the 15 degree ramp in Figure 13. The black data points represent pressure tap measurements taken from the cross-sectional center of the ramp, the red from the cross-sectional left of the ramp as seen by the flow direction, and the blue from the cross-sectional right.

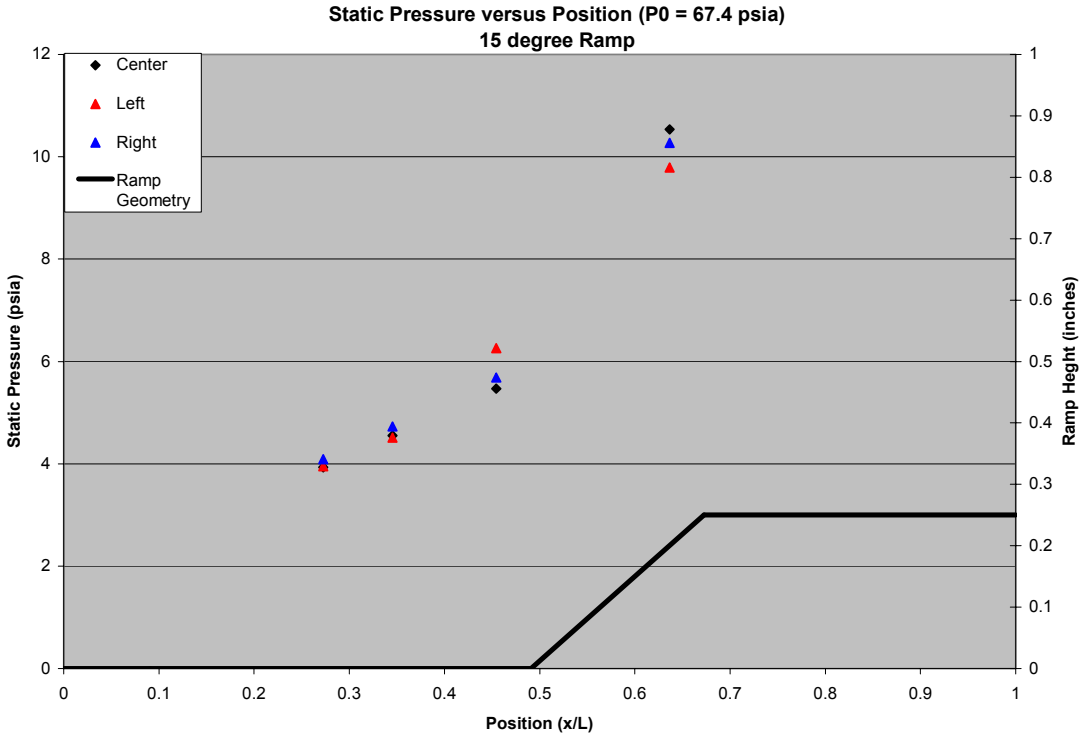

Figure 13: Transverse Pressure Data for the 15 degree Ramp

The plot shows that the pressure was not consistent across the width of the ramp. Because the shock and expansion fan should be constant across the width of the ramp, this data shows effects of 3-dimensional interfering. However because the data points show no trends in terms of which points are higher and which are lower, little can be determined besides the assumption that shocks from the screws, boundary layer interferences, and small inconsistencies in the nozzle geometry cause differences along the width of the flow pressure profile in magnitudes up to 8.5%. Plots for both 25 degree runs further support this inference assumption and can be seen in Appendix Figures A4 and A5.

To examine the behavior of the experimental flow as compared to the theoretical values, the shock and expansion properties of theoretical flow had to be calculated. This was

done using equations 4, 5, 6, and 7 and the process as described in the background section. Figure 14 shows a comparison of the experimental and the theoretical data.

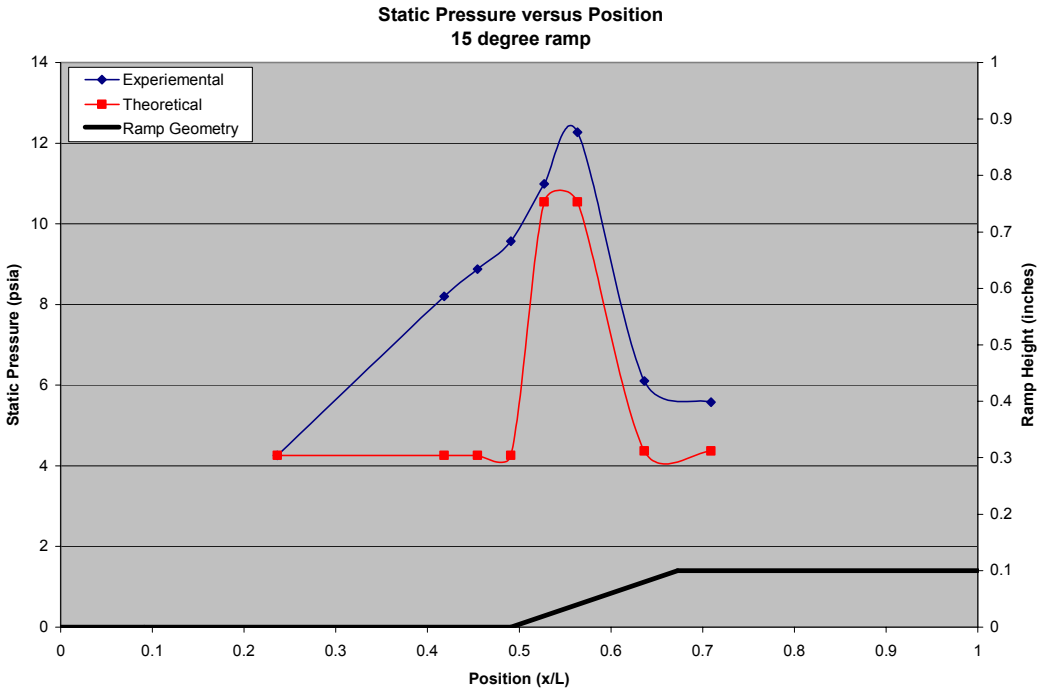

Figure 14: Experimental versus Theoretical Static Pressure distribution

While the experimental behavior does behave in the general fashion that it should, if does not closely resemble the theoretical behavior. This can be attributed mainly to the separation bubble created by the large turning angle. This moves the oblique shock well ahead of its theoretical location. Another large discrepancy is the gradual change in static pressure through the shock rather than the expected discontinuous jump. This can be attributed to the separation bubble having an effect on the strength and continuity of the shock. The data over the expansion fan shows the expected trend and values are off in magnitude only due to the incorrect incoming Mach from the experimental oblique shock.

6.3 Effect of Stagnation Pressure on Shock and Boundary Layer

On the second day, the effects of the plenum chamber stagnation pressure and back pressure were examined for each ramp geometry. Using a vacuum in the downstream end of the tunnel, the back pressure could be pumped from ambient pressure, 14.6 psia, to as low as 6 psia. With a lower back pressure the plenum chamber stagnation pressure could effectively be reduced to as low as 39 psia to get a greater range of stagnation pressures. As stated in the lab manual, the changing back pressure should not affect the nozzle in any way other than allowing a lower stagnation pressure. To demonstrate this assumption, static pressure data was taken for varying back pressures while holding the stagnation pressure constant. Because of the difficulty in obtaining a desired stagnation

pressure with accuracy, the stagnation pressure ratio, static pressure over stagnation pressure, is used to normalize the plot. A plot of the stagnation pressure ratio versus the ramp position for varying back pressures can be seen in Figure 15.

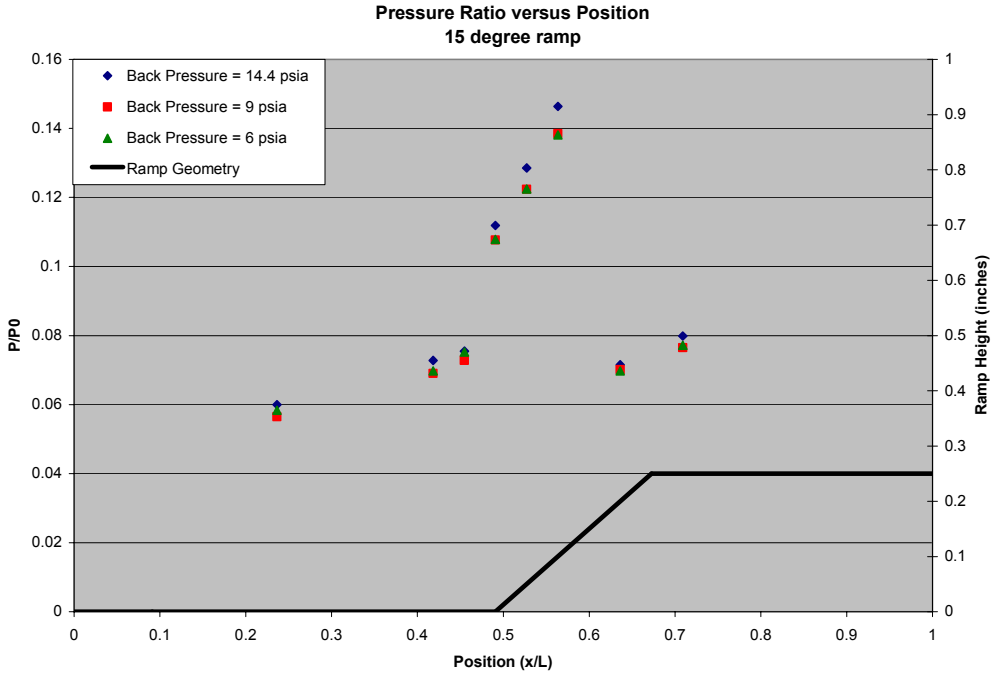

Figure 15: Pressure Ratio versus Ramp Position for varying Back Pressures

As expected, the stagnation pressure ratios match up with a moderately good degree of accuracy. Having shown that the back pressure does not effect the pressure distributions, stagnation pressures with varying back pressures can now be compared. Figure 16 shows a plot of static pressure versus the position for varying stagnation pressure ratios on the 15 degree ramp.

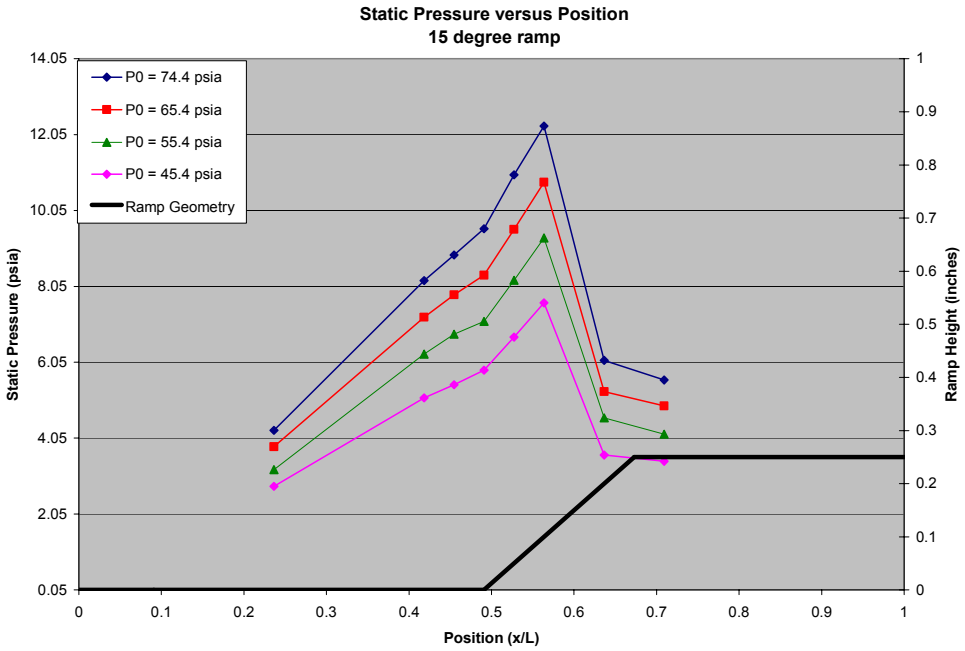

Figure 16: 15° Ramp Static Pressures for varying Stagnation Pressures

The obvious observation is that as the stagnation pressure rises, the static pressure rises. Also seen is that the shock and expansion fans all occur at the same point for all stagnation pressure. Because of a lack of data points, the shock point is hard to visualize, however a visual analysis shows that extending each of the slopes back would lead them to meet at approximately the free stream static pressure. These observations indicate that the stagnation pressure has no effect on the size of the separation bubble or the expansion fan, just the magnitude of the flow going into and out of each component. Because the Mach number is dependent on the stagnation pressure ratio as seen in equation 1, the stagnation pressure ratio is a proportional indication of Mach number. Therefore to examine if the stagnation pressure affects the Mach number, the stagnation pressure ratio will be examined versus the stagnation pressure. This plot is seen for the 15 degree ramp in Figure 17. The plot shows nearly identical points indicating that the Mach number is completely independent of the stagnation pressure.

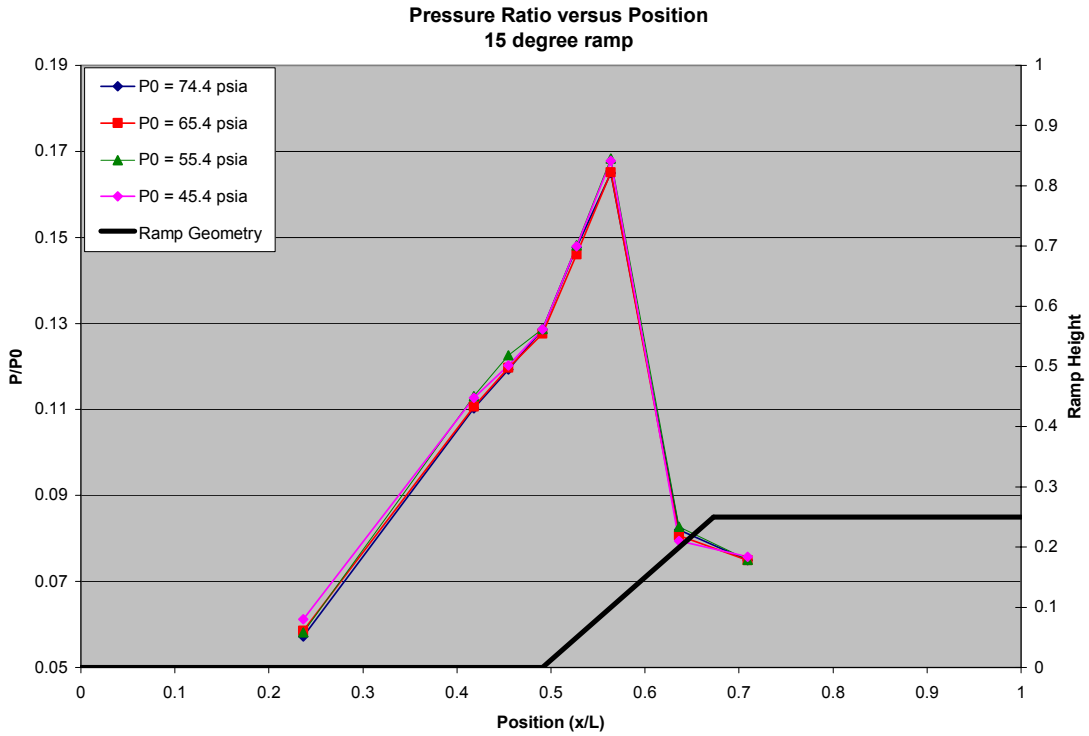

Figure 17: Pressure Ratio versus Position for varying Stagnation pressures

The static pressure versus position plots for the 25 degree ramps can be seen in Figures A6 and A7 in the appendix. Again the same trend is observed, as the stagnation pressure increases the static pressure increases but the stagnation pressure ratios stay constant.

Schlieren images taken for these tests are shown in the Appendix. No significant changes were noticed in the flow for varying stagnation or downstream pressures. For this reason, they have been excluded from the body of this report.

6.4 Oil Flow Visualization

The last objective was to study the flow using oil visualization. Each ramp was tested at two different stagnation pressures. Pictures were taken of each ramp before and after each test. A picture was also taken of the tunnel wall to show the shock yielding a total of 18 pictures. It is not necessary to show each picture taken as much of the phenomena were apparent on more than one picture. Therefore, only a select few will be discussed in this report. Also, the quality of digital camera used was not very good. The pictures taken were quite blurry and poorly lit, making it difficult to make comparisons for many of the runs. Figures 18, 19, and 20 show the initial oil arrangement, the picture of the tunnel during the experiment, and the aftermath of the oil visualization for the 15° ramp, respectively.

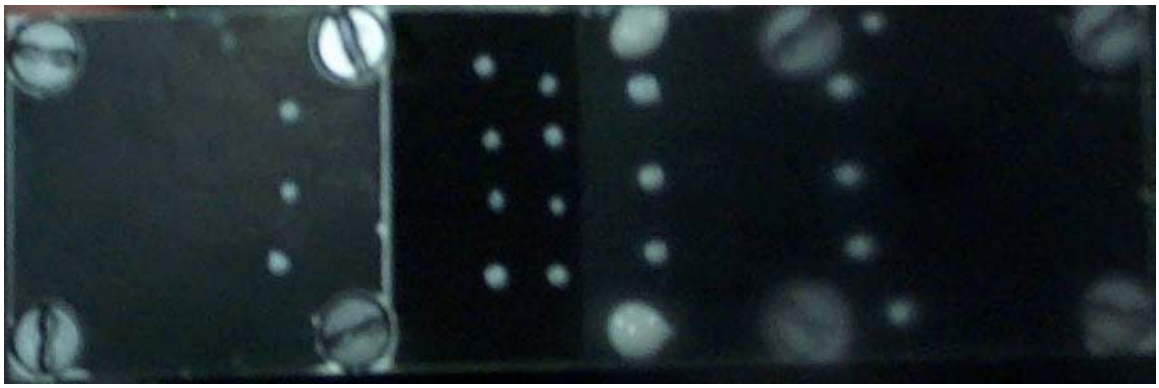

Figure 18: 15° Ramp Oil Flow Untested

Small dots of the oil/paint mixture were used across the surface of the ramp. Two large dots were used near the shock area in order to let the oil flow onto the side walls of the wind tunnel. The effect is seen in Figure 19.

Figure 19: 15°Ramp Oil Flow Shock Visualization

Figure 20: 15°Ramp Oil Flow Post test

Figure 20 shows the movement of the oil during the test. It is evident that the oil placed near the shock did not move longitudinally. The oil placed on the ramp moved longitudinally in the direction of the flow as did the oil at all other locations. The oil on the ramp near the edge also moved in the transverse direction, evidence of 2D effects caused by the wind tunnel and/or screws.

Figure 21 shows the oil placed on the 15° ramp prior to the second test. The second test was run at a reduced stagnation pressure of 35 psig. Figure 22 was taken after the test. There is a clear line where the shock occurs in Figure 20, depicted by the blue line. This clearly shows the effect of the separation bubble on the formation of the shock. Some 2D effects are also seen near the edges of the ramp.

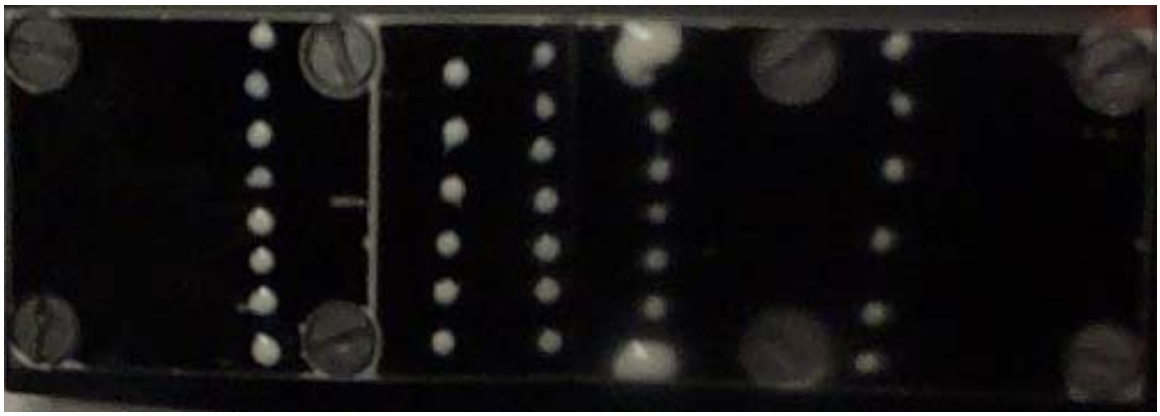

Figure 21: 15°Ramp Oil Flow Untested

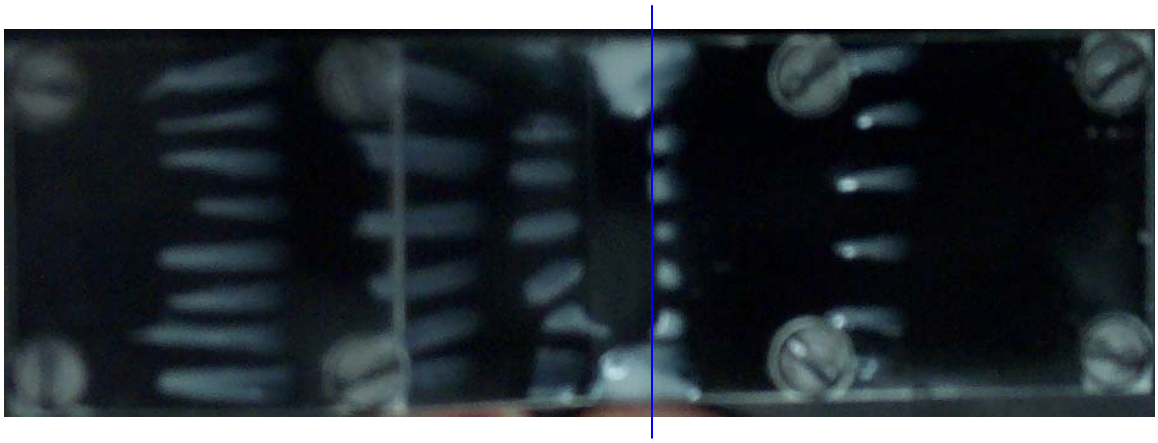

Figure 22: 15°Ramp Oil Flow Post test

7. Discussion and Conclusions

As was expected, there are several sources of error in this experiment. First of all, it's very difficult to compare data collected that shows a definite separation bubble to theoretical calculations that do not take a separation bubble into account. The difference between the measured oblique shock angles and the predicted values differ dramatically. There is no useful comparison to be made when comparing those two sets of data. A comparison can be made between the relative sizes of the separation bubble from ramp to ramp but the fact that a large separation bubble exists, conflicts with the theory behind the calculations, making them almost irrelevant except to say that there is a large difference.

Other sources of error include various shocks seen in the Schlieren images that were not caused by the ramp. Figures 10, 11 and 12 all show several different shocks of unknown origin. These could be caused by the tunnel itself or by the screws on the ramps. Regardless of their origin, they could affect the accuracy of collected data.

Although both the Schlieren and oil flow methods are qualitative compared to the pressure data, they provided some useful information about the flow over the ramp. The separation bubble was evident in all three methods of data collection but was particularly evident from the Schlieren method.

There were a few limitations encountered in this experiment. The side pressure taps were supposed to allow for data collection perpendicular to the flow. However, given that there were only three taps aligned perpendicularly at each cross section point, useful data was not collected. These side data points did not show significant 2D effects nor were they consistent enough to see any patterns. Another limitation was encountered during the oil flow tests. Although the oil flow was able to show some 2D effects and visualize the effects near the shock region, it was not able to provide detailed flow patterns. Because of the thickness of the oil and the method of application, only individual streaks were obtained as opposed to full field oil flow. This could have been modified if time permitted, but it did not. The camera provided for the oil flow pictures was also very inadequate. The pictures taken were very blurry and of low resolution.
There were many things accomplished during this experiment. The Schlieren method was successfully utilized and proved to be a very useful tool to visualize the flow and determine shock angle, separation bubble size, and expansion fan location. Many of the phenomena noticed using the Schlieren method were different than predicted theoretical physics. The separation bubble caused large errors between some of the calculated data and collected data. If this were not visible, it may prove difficult to explain these differences. To a certain extend, the oil flow was successful as well, it was the only method of data collection used that allowed an understanding of the 2D effects present in the flow field; although it could have been improved upon.

Primarily, the objective of this experiment was to learn how to operate the supersonic wind tunnel and associated equipment, use the Schlieren and oil flow visualization methods, and understand the reasons for differences between collected data and theory. This objective was very successful.

9. References

"1.Supersonic Wind Tunnel." AAE520 Background Information.
Purdue University. Jan 19th, 2004.

Bies, C.J. and Bixby, G.A., "Lab 2: Supersonic Shock and Flow Visualization."
Purdue University AAE 520, Spring 2004.

Schneider, S.P., "Introduction to Shock/BL Interaction Lab."
AAE520. Purdue University. Jan 19th, 2004.

http://142.26.194.131/aerodynamics1/High-Speed/oblique_shock_waves.htm

10. Appendix

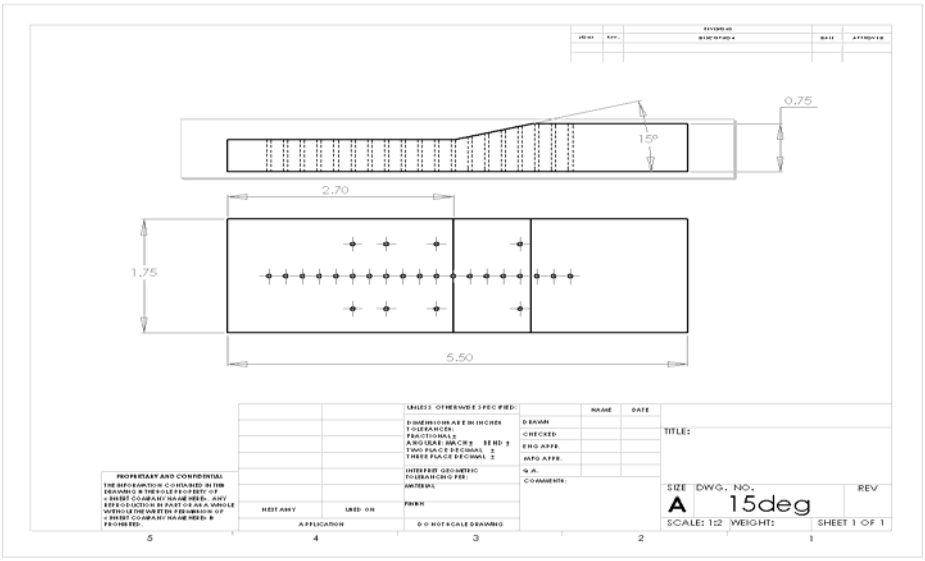

Figure A1: 15° Ramp Schematic

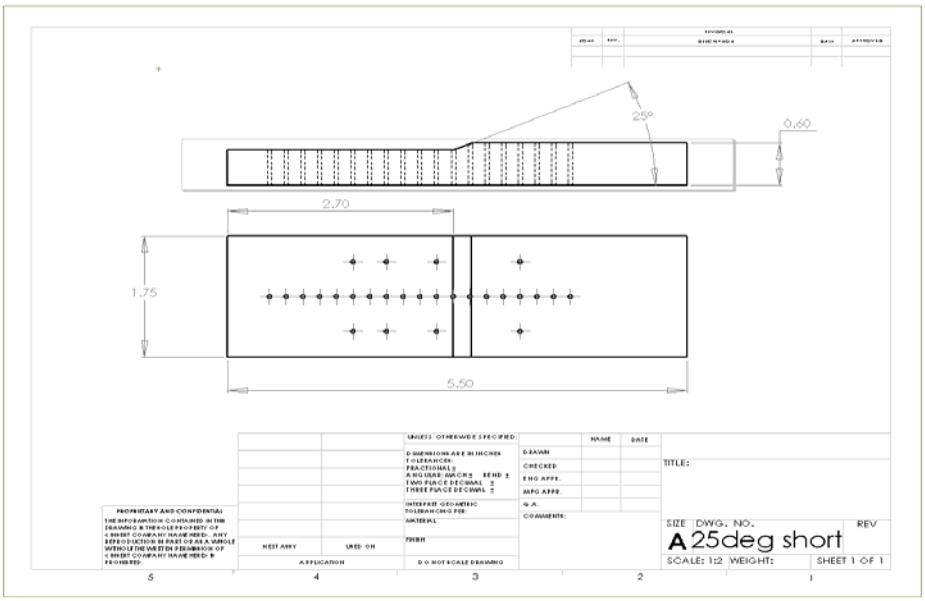

Figure A2: 25° Short Ramp Schematic

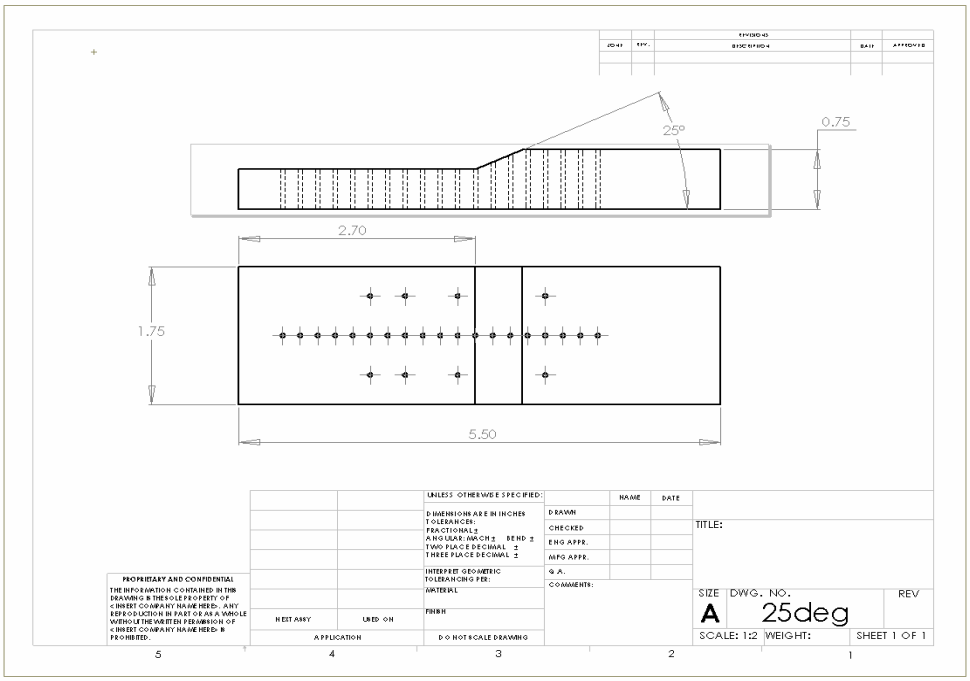

Figure A3: 25° Long Ramp Schematic

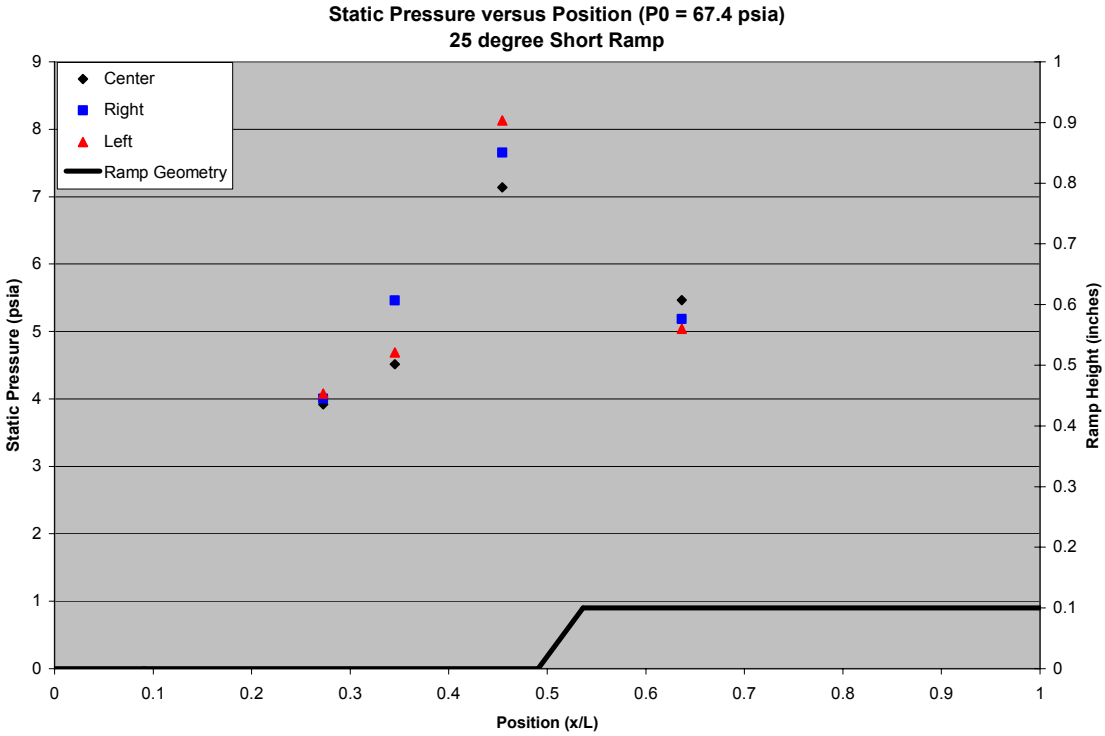

Figure A4: Transverse Pressure Data for the 25 degree Short Ramp

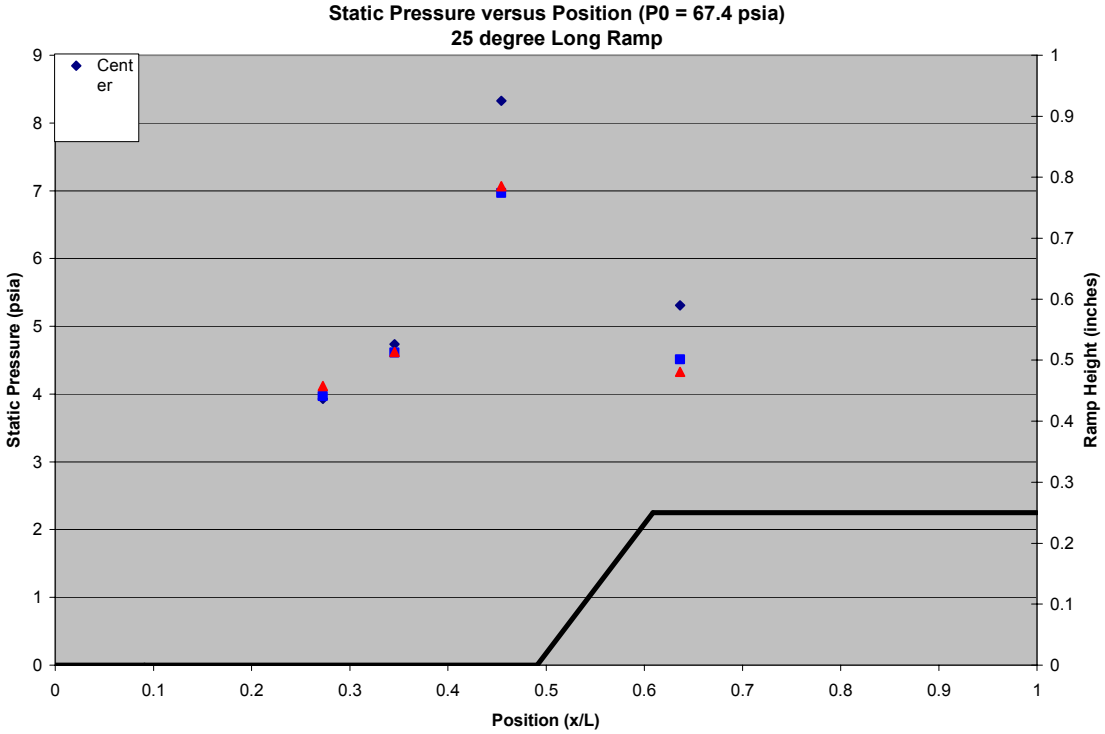

Figure A5: Transverse Pressure Data for the 25 degree Long Ramp

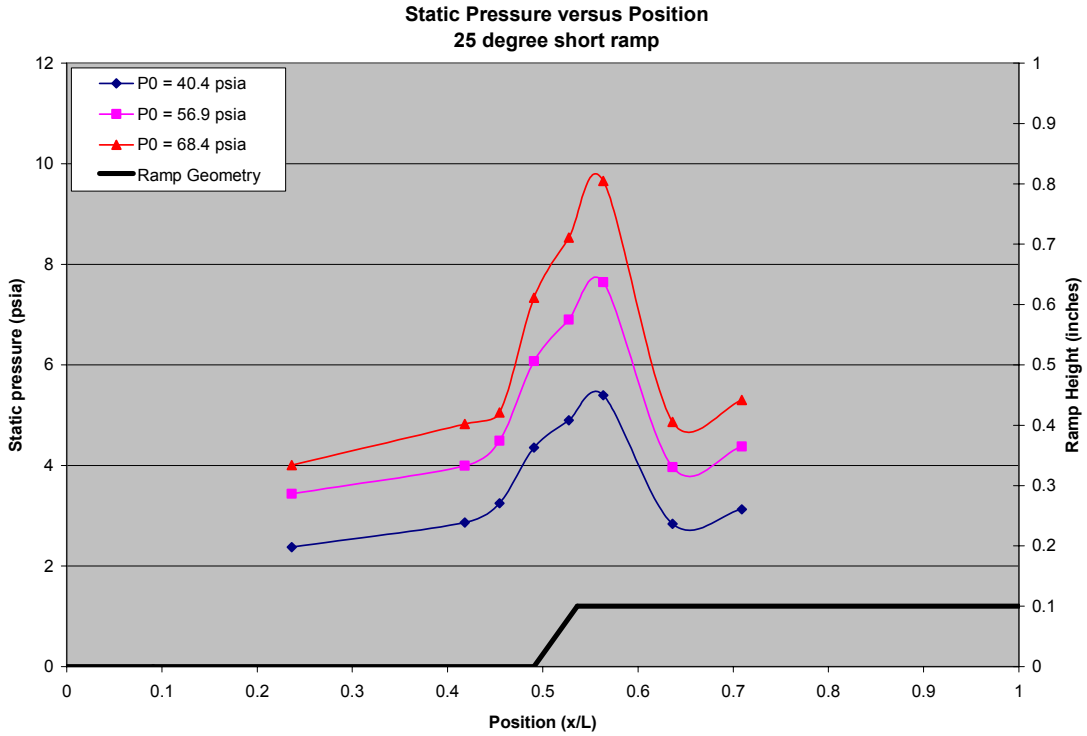

Figure A6: 25° Short Ramp Static Pressures for varying stagnation pressures

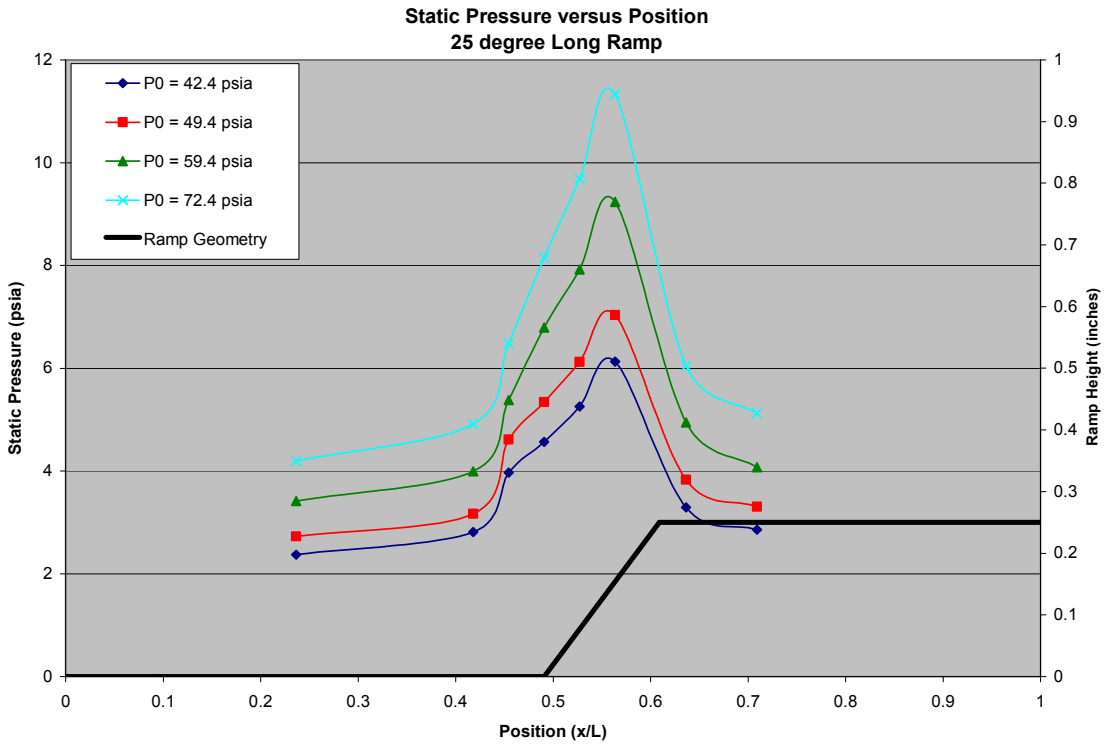

Figure A7: 25° Long Ramp Static Pressures for varying stagnation pressures

10.1 Sample Calculations

- Mach Number Calculated From Pressure Ratio

Given $\frac{P_0}{P} = \left(1 + \frac{\gamma - 1}{2} \cdot M^2\right)^{\frac{\gamma}{\gamma - 1}}$ $P_0 = 67.6$ $P = 6.18$ $\gamma = 1.4$

Find M

$$\frac{67.6}{6.18} = \left(1 + \frac{0.4}{2} \cdot M^2\right)^{\frac{1.4}{0.4}}$$

$$10.39 = \left(1 + 0.2 \cdot M^2\right)^{3.5}$$

$$10.39^{\frac{1}{3.5}} = 1 + 0.2M^2$$

$$1.952 = 1 + 0.2M^2$$

$$\sqrt{\frac{1.952 - 1}{0.2}} = M \qquad M = 2.182$$

-Mach Number Calculated From Area Ratio

Given

$$\left(\frac{A}{Astar}\right)^2 = \frac{1}{M^2}\cdot\left[\frac{2}{\gamma+1}\cdot\left(1+\frac{\gamma-1}{2}\cdot M^2\right)\right]^{\frac{\gamma+1}{\gamma-1}}$$

A = 1.628 Astar = 0.796 γ = 1.4

Find M using iterative process or iterative solver (TI-89 was used)

Guess M = 2.222

$$4.183 = \frac{1}{2.222^2}\cdot[0.833\cdot(1.987)]^6$$

4.183 = 4.165 guess new M

After iteration, M was found

M = 2.223

-Oblique Shock Angle Calculation

Given $\cot(\theta) = \tan(\beta)\cdot\left[\frac{6\cdot(M_1)^2}{5\cdot\left[(M_1)^2\cdot\sin^2(\beta)-1\right]}-1\right]$ $M_1 = 2.5$ $\theta = 15\text{deg}$

Find β β must be found iteratively
first guess of β = 35deg

$$3.732 = 0.7\cdot\frac{6\cdot(2.5)^2}{5\cdot\left(2.5^2\cdot 0.574^2-1\right)}-1$$

3.732 = 4.272 incorrect β guess, iterate

After iteration β = 36.9 deg

-M2 Calculation

Given $\left(M_2\right)^2\cdot\left(\sin\left(\beta-\theta\right)\right)^2=\dfrac{1+\dfrac{\gamma-1}{2}\cdot\left(M_1\right)^2\cdot\sin\left(\beta\right)^2}{\left[\gamma\cdot\left(M_1\right)^2\cdot\sin\left(\beta\right)^2\right]-\dfrac{\gamma-1}{2}}$ $M_1=2.5$ $\theta=15\text{deg}$ $\gamma=1.4$ $\beta=36.9\text{deg}$

Find M2

$$\left(M_2\right)^2\cdot 0.357^2=\frac{1+0.2\cdot 2.5^2\cdot 0.3605}{1.4\cdot 2.5^2\cdot 0.3605-0.2}$$

$$\left(M_2\right)^2\cdot 0.1391=0.491$$

$$M_2=1.879$$

-P02/P01 Pressure Ratio Calculation

Given $\dfrac{P_{02}}{P_{01}}=\left[\dfrac{6\cdot\left(M_1\right)^2\cdot\sin\left(\beta\right)^2}{\left(M_1\right)^2\cdot\sin\left(\beta\right)^2+5}\right]^{\frac{7}{2}}\cdot\left[\dfrac{6}{7\cdot\left(M_1\right)^2\cdot\sin\left(\beta\right)^2-1}\right]^{\frac{5}{2}}$ $M_1=2.5$ $\beta=36.9\text{deg}$

Find P02/P01

$$\frac{P_{02}}{P_{01}}=\left[\frac{6\cdot(2.5)^2\cdot 0.3605}{(2.5)^2\cdot 0.3605+5}\right]^{\frac{7}{2}}\cdot\left[\frac{6}{7\cdot(2.5)^2\cdot 0.3605-1}\right]^{\frac{5}{2}}$$

$$\frac{P_{02}}{P_{01}}=(1.86385)^{\frac{7}{2}}\cdot(0.40618)^{\frac{5}{2}}$$

$$\frac{P_{02}}{P_{01}}=0.929$$

10.2 Schlieren Images

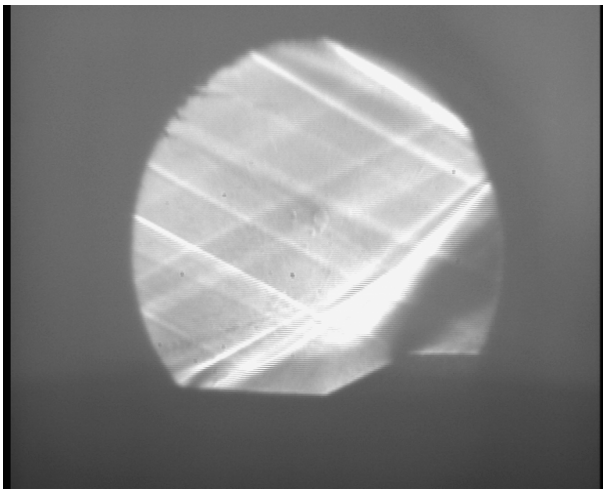

Figure A8 – P0=74.5psia Pd=9psia

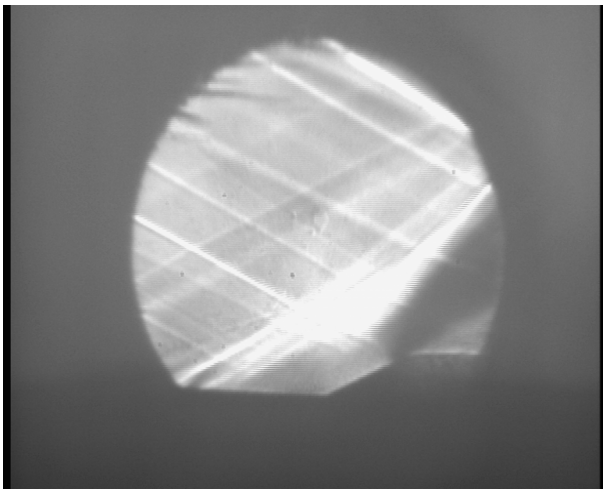

Figure A9 – P0=74.3psia Pd=5.4psia

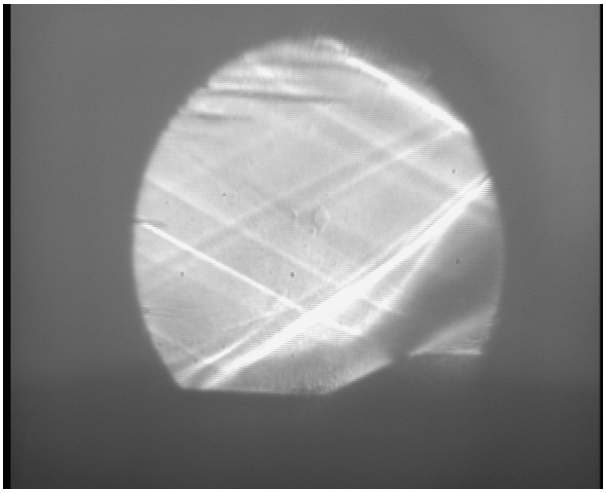

Figure A10 – P0=44.5psia Pd=14.5psia

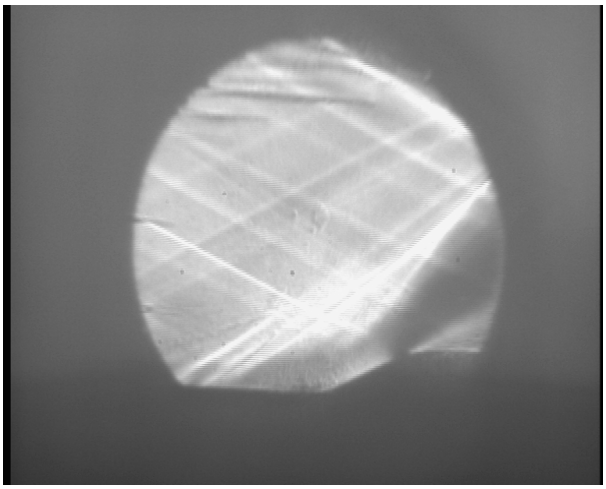

Figure A11 – P0=54.5psia Pd=9psia

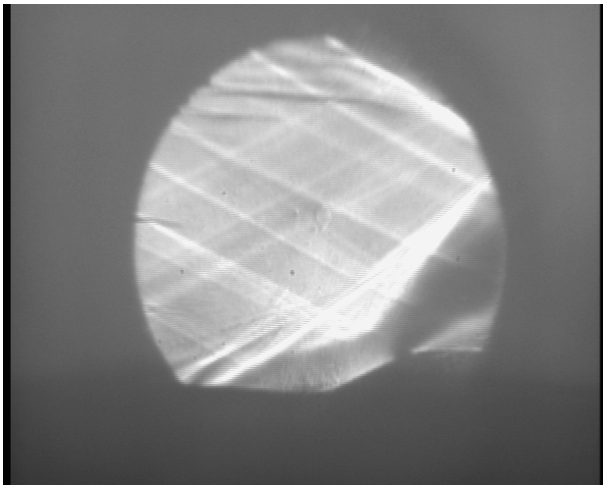

Figure A12 – P0=65.5psia Pd=14.5psia

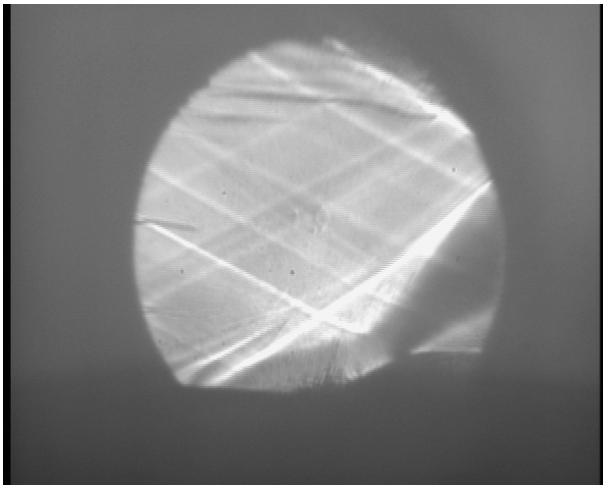

Figure A13 – P0=60.5psia Pd=9psia

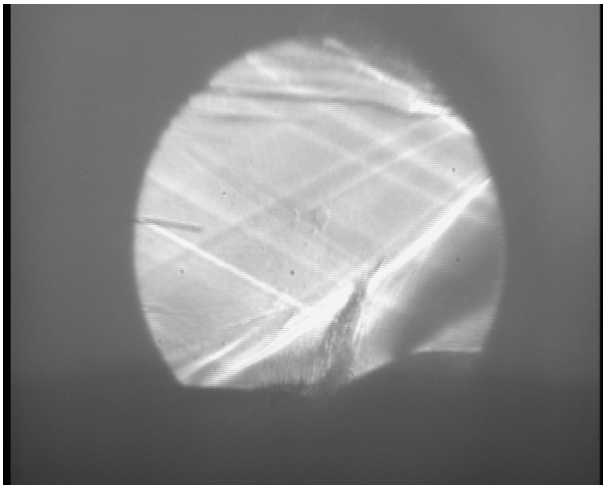

Figure A14 – P0=48.5psia Pd=6psia

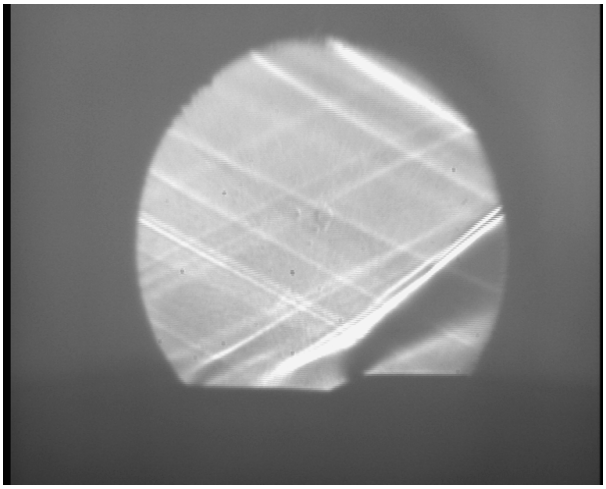

Figure A15 – P0=57psia Pd=14.5psia

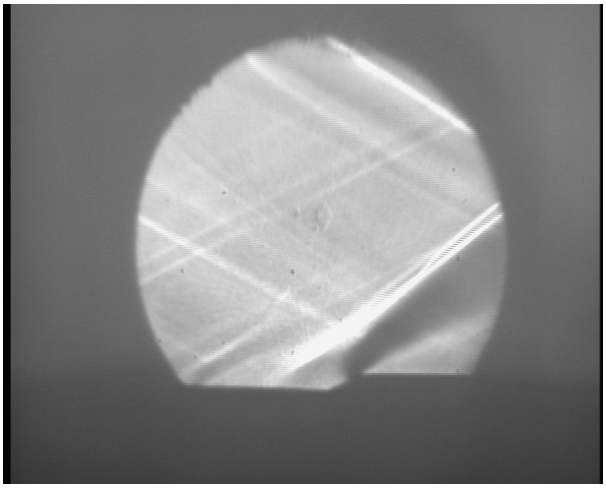

Figure A16 – P0=40.5psia Pd=14.5psia

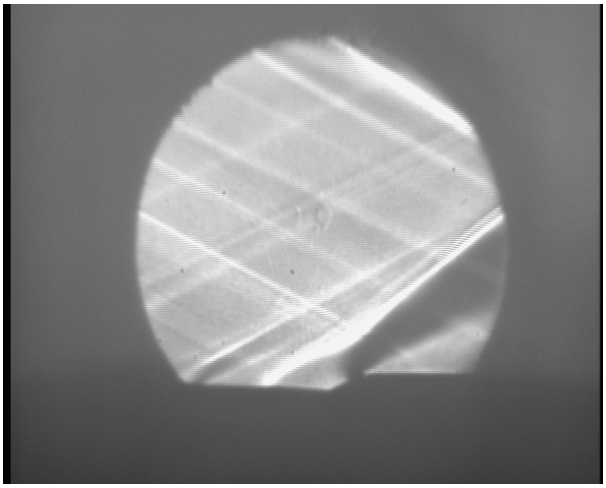

Figure A17 – P0=68.5psia Pd=14.5psia

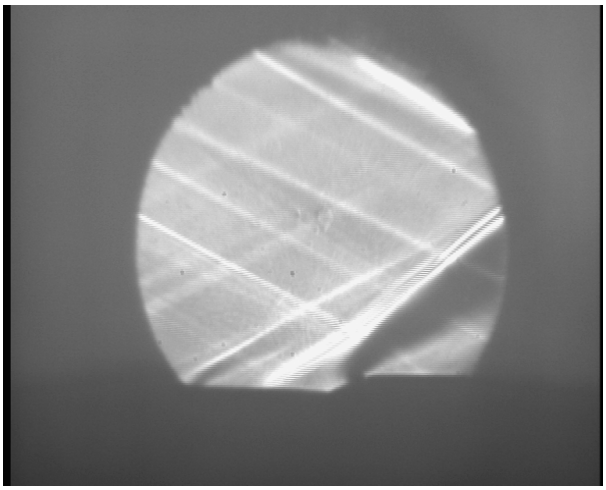

Figure A18– P0=70.5psia Pd=14.5psia

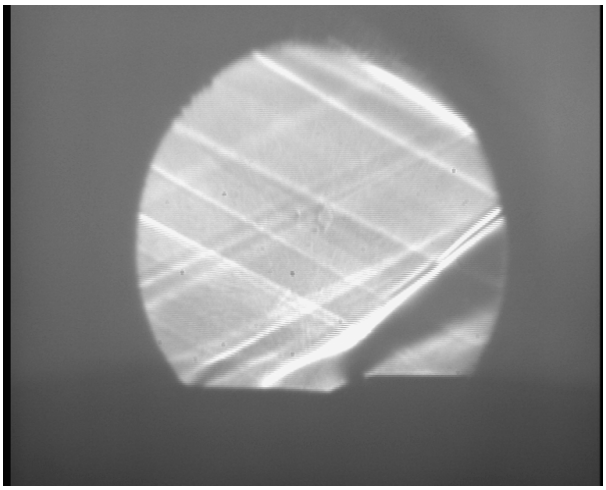

Figure A19 – P0=70.5psia Pd=6psia

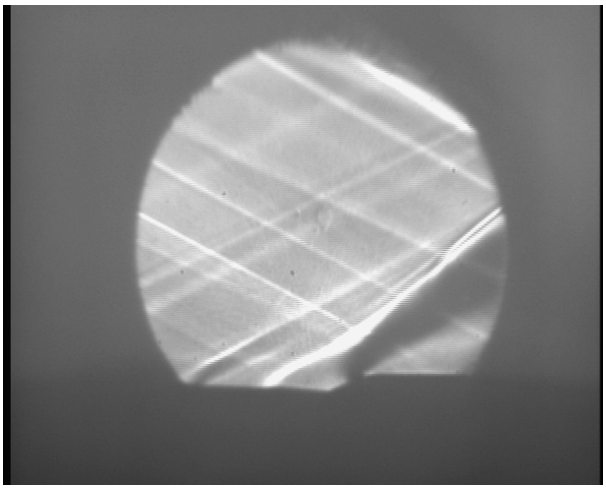

Figure A20 – P0=70.5psia Pd=9psia

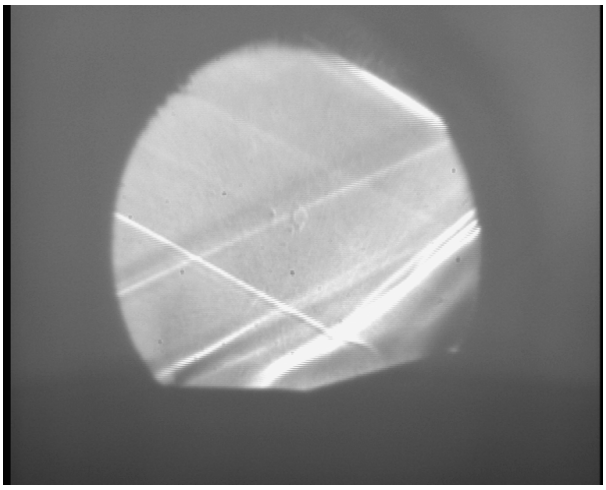

Figure A21 – P0=69.5psia Pd=6psia

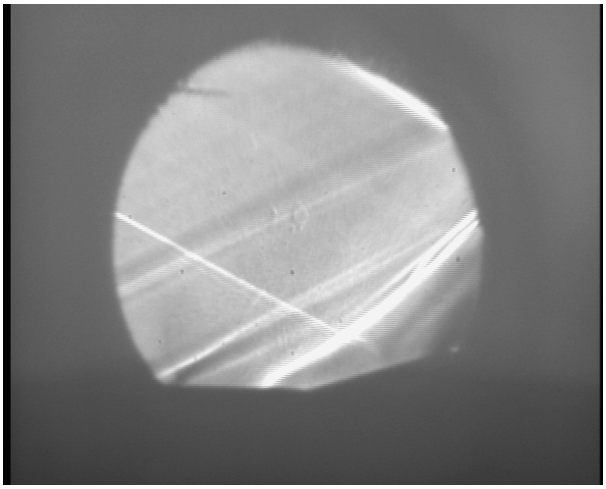

Figure A22 – P0=74.5psia Pd=9psia

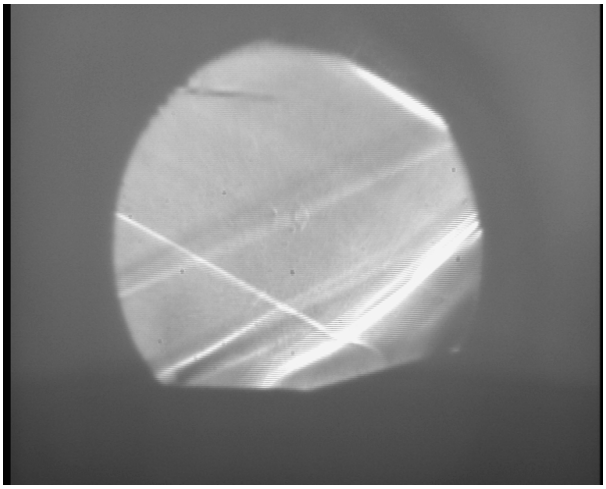

Figure A23 – P0=72.5psia Pd=14.5psia

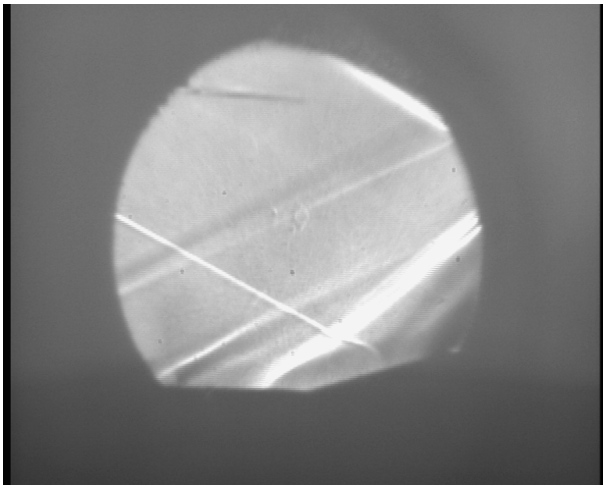

Figure A24 – P0=59.5psia Pd=14.5psia

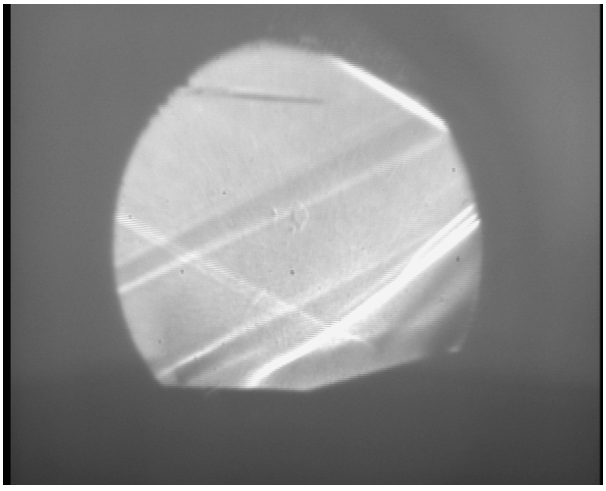

Figure A25 – P0=49.5psia Pd=14.5psia